Advanced 3D Monte Carlo Algorithms for Biophotonic and Medical Applications

Lewis McMillan

University of
St Andrews

This thesis is submitted in partial fulfilment for the degree of
PhD
at the
University of St Andrews

March 2019

Declaration

I, Lewis McMillan, hereby certify that this thesis, which is approximately ***** words in length, has been written by me, that it is the record of work carried out by me, or principally by myself in collaboration with others as acknowledged, and that it has not been submitted in any previous application for a higher degree.

I was admitted as a research student in September 2015 and as a candidate for the degree of PhD in September 2015; the higher study for which this is a record was carried out in the University of St Andrews between 2015 and 2019.

Date . . . .   Signature of candidate . . . .

I hereby certify that the candidate has fulfilled the conditions of the Resolution and Regulations appropriate for the degree of PhD in the University of St Andrews and that the candidate is qualified to submit this thesis in application for that degree.

Date . . . .   Signature of supervisor . . . .

Date . . . .   Signature of supervisor . . . .

Abstract

Lorem ipsum dolor sit amet, consectetuer adipiscing elit. Ut purus elit, vestibulum ut, placerat ac, adipiscing vitae, felis. Curabitur dictum gravida mauris. Nam arcu libero, nonummy eget, consectetuer id, vulputate a, magna. Donec vehicula augue eu neque. Pellentesque habitant morbi tristique senectus et netus et malesuada fames ac turpis egestas. Mauris ut leo. Cras viverra metus rhoncus sem. Nulla et lectus vestibulum urna fringilla ultrices. Phasellus eu tellus sit amet tortor gravida placerat. Integer sapien est, iaculis in, pretium quis, viverra ac, nunc. Praesent eget sem vel leo ultrices bibendum. Aenean faucibus. Morbi dolor nulla, malesuada eu, pulvinar at, mollis ac, nulla. Curabitur auctor semper nulla. Donec varius orci eget risus. Duis nibh mi, congue eu, accumsan eleifend, sagittis quis, diam. Duis eget orci sit amet orci dignissim rutrum.

Nam dui ligula, fringilla a, euismod sodales, sollicitudin vel, wisi. Morbi auctor lorem non justo. Nam lacus libero, pretium at, lobortis vitae, ultricies et, tellus. Donec aliquet, tortor sed accumsan bibendum, erat ligula aliquet magna, vitae ornare odio metus a mi. Morbi ac orci et nisl hendrerit mollis. Suspendisse ut massa. Cras nec ante. Pellentesque a nulla. Cum sociis natoque penatibus et magnis dis parturient montes, nascetur ridiculus mus. Aliquam tincidunt urna. Nulla ullamcorper vestibulum turpis. Pellentesque cursus luctus mauris.

Acknowledgements

Lorem ipsum dolor sit amet, consectetuer adipiscing elit. Ut purus elit, vestibulum ut, placerat ac, adipiscing vitae, felis. Curabitur dictum gravida mauris. Nam arcu libero, nonummy eget, consectetuer id, vulputate a, magna. Donec vehicula augue eu neque. Pellentesque habitant morbi tristique senectus et netus et malesuada fames ac turpis egestas. Mauris ut leo. Cras viverra metus rhoncus sem. Nulla et lectus vestibulum urna fringilla ultrices. Phasellus eu tellus sit amet tortor gravida placerat. Integer sapien est, iaculis in, pretium quis, viverra ac, nunc. Praesent eget sem vel leo ultrices bibendum. Aenean faucibus. Morbi dolor nulla, malesuada eu, pulvinar at, mollis ac, nulla. Curabitur auctor semper nulla. Donec varius orci eget risus. Duis nibh mi, congue eu, accumsan eleifend, sagittis quis, diam. Duis eget orci sit amet orci dignissim rutrum.

Nam dui ligula, fringilla a, euismod sodales, sollicitudin vel, wisi. Morbi auctor lorem non justo. Nam lacus libero, pretium at, lobortis vitae, ultricies et, tellus. Donec aliquet, tortor sed accumsan bibendum, erat ligula aliquet magna, vitae ornare odio metus a mi. Morbi ac orci et nisl hendrerit mollis. Suspendisse ut massa. Cras nec ante. Pellentesque a nulla. Cum sociis natoque penatibus et magnis dis parturient montes, nascetur ridiculus mus. Aliquam tincidunt urna. Nulla ullamcorper vestibulum turpis. Pellentesque cursus luctus mauris.

Contents

Abbreviations

CVD cardiovascular disease.

CVDs cardiovascular diseases.

MCRT Monte Carlo radiation transfer.

NM Nelder-Mead.

List of Figures

Chapter 1

AmoebaMCRT, modelling autofluorescence in skin for novel biomarkers of cardiovascular disease

1.1 Introduction

Cardiovascular diseases (CVDs) are the leading cause of death in the world [1]. It is estimated that around 18 million people dies in 2016 from CVDs, accounting for 31% of global deaths [1]. Despite decreasing burden of cardiovascular disease (CVD) in the UK, it was still the number two cause of death in the Uk in 2014 [2]. Traditional markers for do not fully explain incidence of disease. Therefore research has moved to examining more novel biomarkers for detecting the disease. Amongst these novel biomarker, the autofluorescence response of tissue is of much interest. Changes in the autofluorescencent response of tissue has been linked to cancer, Alzheimers, diabetes and CVDs. Autofluorescence is particularly attractive as a biomarker for these disease as they requires no exogenous dyes, which can be toxic, non-specific, or interfere with biological function [3].

Despite their appeal, using these novel biomarkers to diagnose and asses disease risks, information on the location of fluorescence, which fluorophores contribute to the signal and how much, how much the optics of tissue affect the signal, and the variability of the signal over small and large length scales.

Fluorophores in the Skin

There are various different molecules and compounds responsible for the autofluorescence response in tissue. These include NADH (nicotinamide adenine dinucleotide), structural proteins like collagen and elastin, aromatic amino acids (tyrosine and tryptophan), porphyrins, and FAD (flavin adenine nucleotide).
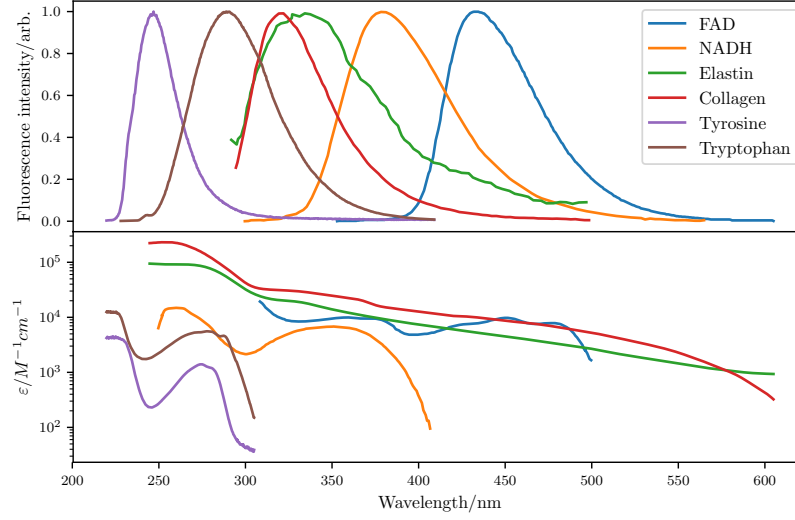
Figure 1.1: *Top) Shows the fluorescent emission for the various different fluorophores. Bottom) Extinction coefficients for a selection fluorophores found in the skin.*

1.2 Skin Model

So far in this thesis all tissue models have been simplified, by assuming that tissue is a homogeneous structure with uniform optical properties. However this is not the case in reality. Tissue is very un-homogeneous, with non-uniform optical properties. However, to create a one to one model of tissue in a simulation is impractical due to the resolution required to resolve all the constituent parts of the tissue down to the cell level. Therefore we need to make a compromise between reality and what is possible to model efficiently. To this end the section presents a 5 layer model of human skin.

Dermatologists split the skin into several layers based upon the morphology, function and contents of each layer. The layers named from outer layer to inner most layer: Stratum corenum, Stratum lucidum, Stratum granulosum, Stratum spinosum, Stratum basale, Papillary dermis, Reticular dermis and Hypodermis. As not all these layers are optically distinct or are too small to model, we therefore simplify the layers into just 5 layers: Stratum Corneum, Epidermis Papillary Dermis, Reticular Dermis, and Hypodermis, see Fig. 1.2.

Each of these layers have various amounts of chromophores and scatterers. To accurately model these various chromophores and scatterers, and therefore the skin, we must discuss the chemical makeup and spatial structure of the skin.

Stratum Corenum

The outer most layer of the skin is the Stratum corenum. This layer mostly consists of dead skin cells (keratinocytes). The function of this layer is to be a protection barrier to prevent damage, infection and diffusion of unwanted chemicals.

Epidermis

Below the Stratum corenum is the epidermis. The epidermis consist of several layers that are optically similar so we restrict our model to modelling this as one whole layer. The layers that
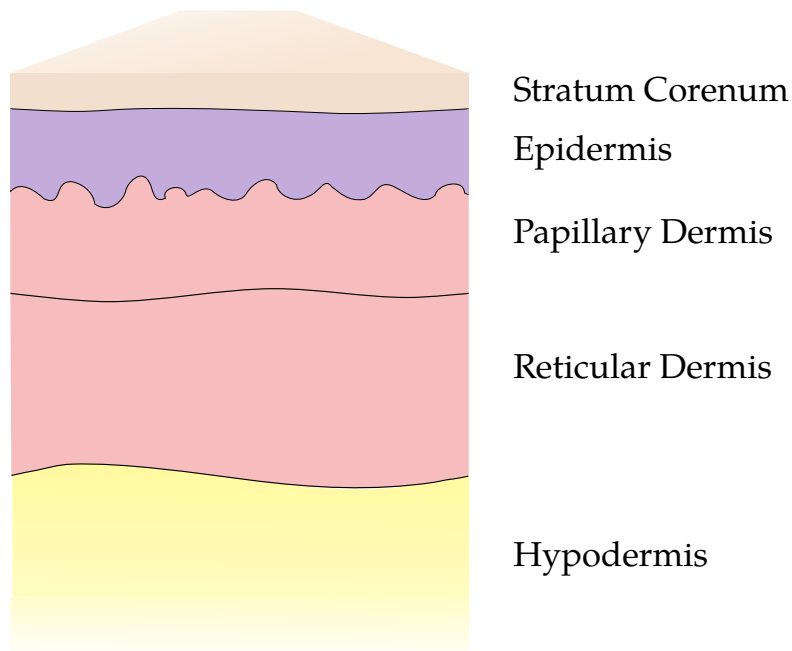
Figure 1.2: *Illustration of our 5 layer skin model.*

make up the epidermis are the stratum basale, stratum spinosum, stratum granulosum, and the stratum lucidum*. The purpose of the epidermis is as before to provide a protective barrier to the underlying layers. The epidermis contains melanin which protects the stem cell keratinocytes which divide to form keratinocyte which form much of the upper layers of the skin. In the stratum basale there is also melanocytes which produce the pigment melanin which is responsible for the color of the skin, and providing some protection from harmful UV light. Other types of cells found in the epidermis are Langerhans cells and Merkel cells which are part of the immune system and nervous system respectively.

Dermis

The dermis is split into three different layers in our model: the papillary dermis, reticular dermis and the hypodermis.

The papillary dermis has blood
The reticular dermis has blood
The hypodermis consists of fat and

Optical Properties

With a discussion of what makes up the skin, and what molecules contribute to the skins optical properties, this section gives an account of how our skin model models the optical properties of skin.

To model blood, we first split blood into its deoxygenated and oxygenated components. This is done as the absorption coefficient differs between the two types of blood. We mix these two

---

*The stratum corenum is usually part of the epidermis, however as its optical properties are different than that of the epidermis we model it as a separate layer.

groups using the tissue oxygenation coefficient S. Blood absorption spectra are taken from S. Prahl [4].

$$\mu_{a,oxy/deoxy} = 150 \; \ln 10 \; \frac{\epsilon}{64458} \qquad (1.1)$$

$$\mu_{a,b}(\lambda) = SO_2\mu_{a,Oxy} + (1 - SO_2)\mu_{a,DeOxy} \qquad (1.2)$$

The next chromophores are bilirubin and β-carotene. These chromophores are yellow/ornage pigments. Bilirubin is usually responsible for the yellow skin colour seen in people with jaundice. The absorption coefficients are calculated using the blah The spectra are taken from S. Prahl's compilation of PhotochemCAD data [5,6].

$$\mu_{a,Bilirubin}(\lambda) = \frac{\epsilon_{bilirubin}}{585} \; ln10 \; C_{bilirubin} \qquad (1.3)$$

$$\mu_{a,\beta-Caro}(\lambda) = \frac{\epsilon_{\beta-Caro}}{537} \; ln10 \; C_{\beta-Caro} \qquad (1.4)$$

To model melanin's absorption coefficient we use Eq. (1.6), taken from...

$$\mu_{a,eumel}(\lambda) = 6.66 \times 10^{11} \times \lambda^{-3.33} \qquad (1.5)$$
$$\mu_{a,phomel}(\lambda) = 2.9 \times 10^{15} \times \lambda^{-4.75} \qquad (1.6)$$

Finally we use a base absorption coefficient to model the absorption due to the other parts of the skin that contribute to its optical properties, but individually do not have a large effect. The equation for modelling this was taken from I. Sahdi [7]

$$\mu_{a,b} = 7.84 \times 10^8 \times \lambda^{-3.255} \qquad (1.7)$$

Figure 1.3 shows the absorption spectra for the above chromophores as a function of wavelength.
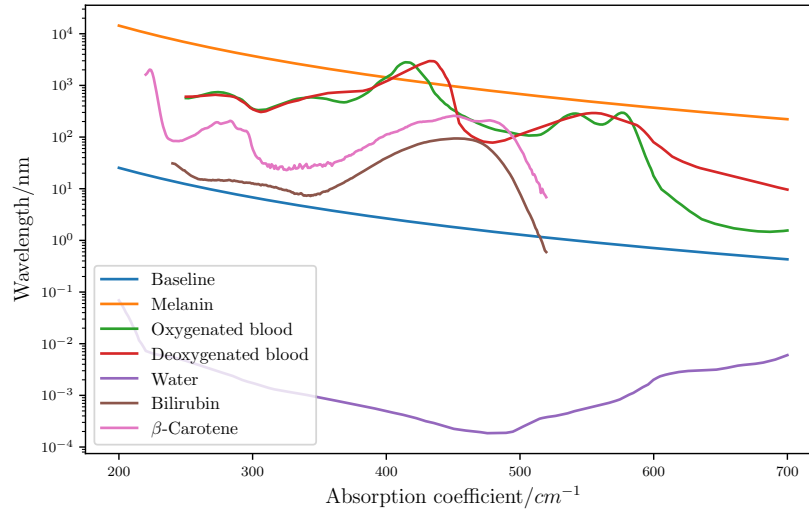

Figure 1.3: *Absorption coefficients for the various chromophores found in skin.*

With the absorption properties of the various chromophores in the skin defined we can now discuss the scattering properties of the skin. As the scattering properties do not vary from layer to layer by too much we use the same equation to describe the scattering coefficient. [8–10].

$$\mu'_s(\lambda) = a'\left(f_{ray}\left(\frac{\lambda}{500(nm)}\right)^4 + (1 - f_{ray})\left(\frac{\lambda}{500(nm)}\right)^{-b_{\text{mie}}}\right) \quad (1.8)$$

$$\mu'_s(\lambda) = 1050.60 \times \lambda^{-0.68} \quad (1.9)$$

Where:

μ'_s is the reduced scattering coefficient $[cm^{-1}]$;
a' is a scaling factor $[cm^{-1}]$;
f_{ray} is the fraction of Raylieigh scattering [-];
λ is the wavelength of light $[m]$;
and b_{mie} is the "scattering power" [-].

Layer	a'/cm^{-1}	f_{ray}	b_{mie}
Epidermis	66.7	0.29	0.69
Dermis	43.6	0.41	0.35

Table 1.1: *Values of the constants for the scattering equations for the different layers of our skin model. Here epidermis represents the stratum corenum and the epidermis, and dermis represents the papillary, reticular and hypodermis in our model.*
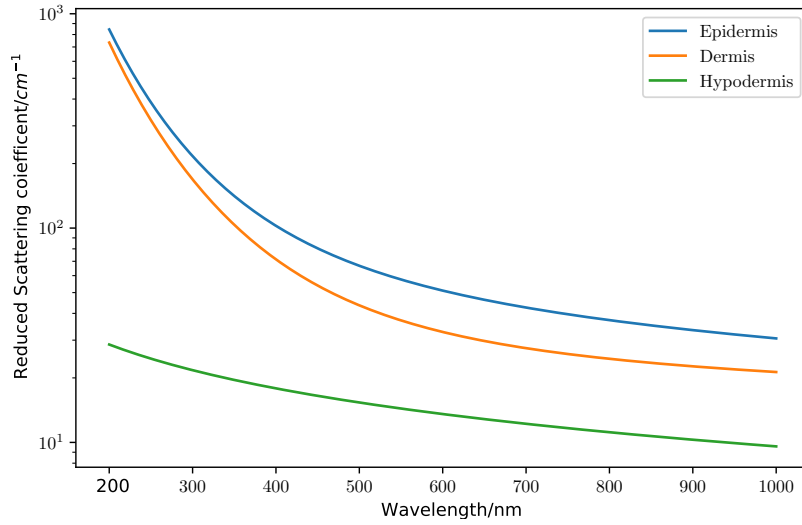

Figure 1.4: *Figure shows the reduced scattering coefficient for the different layers of our skin model.*

$$\mu_{a,strat} = ((0.1 - 0.3 \times 10^{-4} \cdot \lambda) + (0.125(\lambda/10.)) \times \mu_{a,b}(\lambda)) \times (1. - W) + W \cdot \mu_{H_20}(\lambda) \quad (1.10)$$
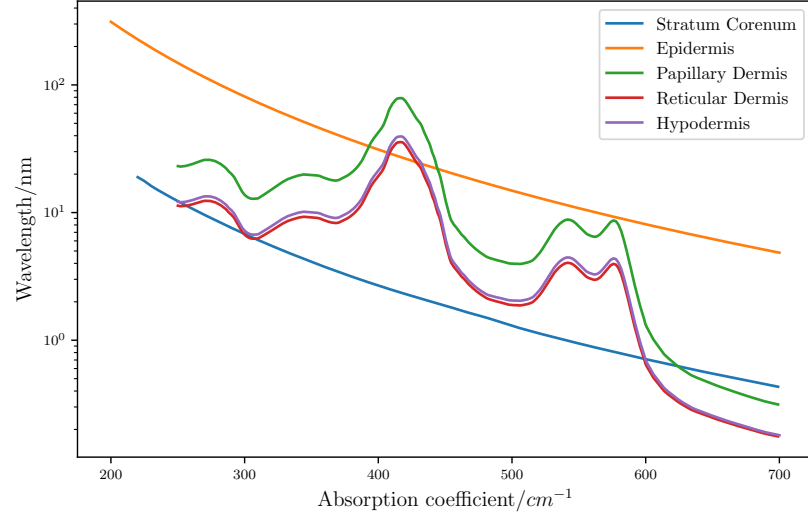
Figure 1.5: *Absorption coefficients for the different layers in the skin.***swap the labels!!!****

Layer	Thickness/ cm	Refractive index	Blood volume/%	Melanin volume/%	Bilirubin/ gL^{-1}	β-Carotene/ gL^{-1}	Water volume/%
Stratum Corenum	0.02	1.50	0.0	0.0	0.0	0.0	0.05
Epidermis	0.08	1.34	0.0	1.0	0.0	2.1e-4	20.0
Papillary Dermis	0.18	1.40	6.0	0.0	0.05	7e-5	50.0
Reticular Dermis	1.82	1.395	4.5	0.0	0.05	7e-5	70.0
Hypodermis	5.90	1.41	5.0	0.0	0.0	0.0	70.0

Table 1.2: *Table of values used for the various concentrations and volumes fraction of the chromophores in the five layer skin model. Values taken from [9, 11–13].*

$$\mu_{a,epi} = (\nu_m \cdot (\mu_{phomel}(\lambda) + \mu_{eumel}(\lambda)) + (\mu_{a,b}(\lambda) + \ln 10 \cdot \mu_{a,\beta-caro}(\lambda) \cdot C_{caro}) \\ \times (1.-\nu_m)) \times (1.-W) + W \cdot \mu_{H_2O}(\lambda) \tag{1.11}$$

$$\mu_{a,pap} = ((S \cdot \mu_{a,oxy}(\lambda) + (1.-S) \cdot \mu_{a,deoxy}(\lambda) + \ln 10 \cdot \mu_{a,\beta-caro}(\lambda) \cdot C_{caro} + \\ \ln 10 \cdot \mu_{a,bili}(\lambda) \cdot C_{bili}) \cdot B + \mu_{a,b}(\lambda) \times (1.-B)) \times (1.-W) + W \cdot \mu_{H_2O}(\lambda) \tag{1.12}$$

$$\mu_{a,hypo} = \tag{1.13}$$

To create our 5 layer skin model, we mix different amounts of the above chromophores to match what appears in each layer. Table 1.2 shows the amount of each chromophore is included in each layer.

1.3 Modelling Fluorescence

Fluroescene is the process in which light of a certain wavelength is incident on a molecule, the molecule absorbs the light and re-emits the light at a new longer wavelength.
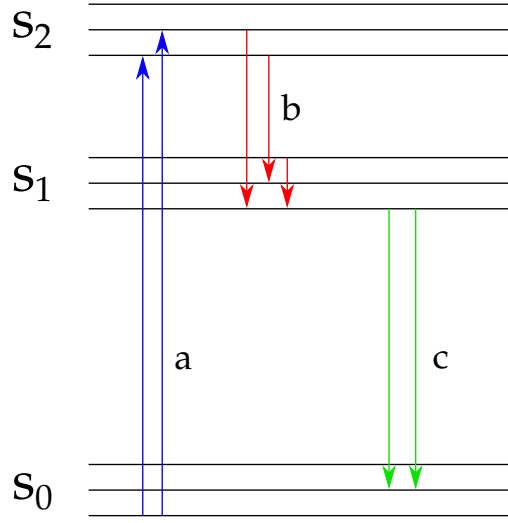
Figure 1.6: *Jablonski diagram for PPIX. a) excitation of the ground state via absorption of a photon, b) non-radiative transition, and c) fluorescence.*

Figure 1.6 shows an example of Jablonski diagram.

To model fluorescence from multiple fluorophores requires a change of the Monte Carlo radiation transfer (MCRT) code presented thus far. This change is to the interaction portion of the algorithm, so that it will now include the option for a packet to undergo fluorescence. To calculate whether a packet absorbs, scatters or fluoresces, first the probability of each of these events must be calculated. Discussion of scattering and absorption (by the bulk medium) was described in **??**. To calculate the probability of fluorescence, we first assume that the quantum yield of the molecule is unity. This is physically unrealistic, however it does not affect the simulations accuracy, as modelling a realistic quantum yield would mean that more packets would be discarded, and thus the signal to noise ration would be worse than if we assume a quantum yield of unity. To calculate the probability of fluorescence, the absorption coefficient of the florescent molecule must be calculated. This is shown in Eq. (1.14):

$$\mu_f = \ln(10)\, C\varepsilon \tag{1.14}$$

Where C is the concentration of the fluorophore, ε is the extinction coefficient of the fluorophore, and $ln(10)$ is the natural logarithm of $10^{\dagger}$.

The next step is to calculate the total attenuation coefficient for a given species as in Eq. (1.15)

$$\mu_{t_i} = \mu_{s_i} + \mu_{a_i} + \mu_{f_i} \tag{1.15}$$

Where as usual μ_a and μ_s are the absorption and scattering coefficients, and μ_f is the fluorescence coefficient as defined in Eq. (1.14). As the absorption coefficient of fluorophores are small in comparison to the medium, and that the absorption coefficient of fluorescent molecules are generally much larger than that of their scattering coefficient, we assume that the scattering coefficient is negligible. Finally we calculate the probability of interacting with a given species using Eq. (1.16)

---

†This factor appears as historically ε was measured in base 10 [8].

$$P_i = \frac{\mu_{t,i}}{\sum\limits_{i=1}^{N} \mu_{t,i}} \tag{1.16}$$

Where P_i is the probability of interacting with the ith species, the numerator is the attenuation coefficient for i^{th} species, and the denominator is the total attenuation coefficient for all the species.

Algorithm 1 shows the process used to determine which species to interact with.

set μ_{tot};
set all P_i's;
set ξ_1;
if $\xi_1 < P_1$ **then**
    set ξ_2;
    if $\xi_2 < a_m$ **then**
        Scatter in medium;
    else
        Absorb in medium;
    end
else if $\xi_1 < P_1 + P_2$ **then**
    Species 1 fluoresces;
else if $\xi_1 < P_1 + P_2 + P_3$ **then**
    Species 2 fluoresces;
else if $\xi_1 < P_1 + P_2 + P_3 + ... + P_n$ **then**
    Species n fluoresces;
else
    Error;
end

Algorithm 1: *An algorithm to determine which species to interact with. P_1 is the probability of interacting with the bulk medium, P_2 to P_n is the probability of interacting with a fluorescent species, a_m is the albedo of the bulk medium, ξ_i is a random number, and μ_{tot} is the total attenuation coefficient of all the species summed.*

This method allows an arbitrary number of fluorophores to be modelled. To ensure that this method works as intended, the method is compared to experimental data taken by Campbell *et al.*.

405 nm light was shone on a cuvette of area 10 $mm \times 10$ mm. The cuvette was filled with Intrlipid 20% diluted with water, and a fluorescent agent Coproporphyrin III. The total volume of this mixture was 6 ml, consisting of 1 ml of Coproporphyrin III, 4.99 ml of water, and 0.0 1ml of Intrlipid 20%, of which 2 ml was pipetted into the cuvette. 405 nm light was shone on the cuvette, and collected via the same fiber, of diameter 600 μm. The fiber has a NA of 0.22. The signal is the recorded by a blah blah blah..

The simulation is setup to mimic the experimental setup. A medium of 10 mm^3 is used with 1 voxel to increase the speed of computation. As before Intralipid is assumed to be wholly scattering with no absorption, so an albedo of 1 is used. Conversely the Coproporphyrin III is wholly absorbing with no scattering. Coproporphyrin III absorption coefficient is as shown along side its emission spectrum in Fig. 1.7. If a photon packets leave the top face of the simulated medium, within the radius of the fiber at an angle the fiber could accept, then the packet is recorded. The simulation is run with 10^7 photons which yielded Fig. 1.8.
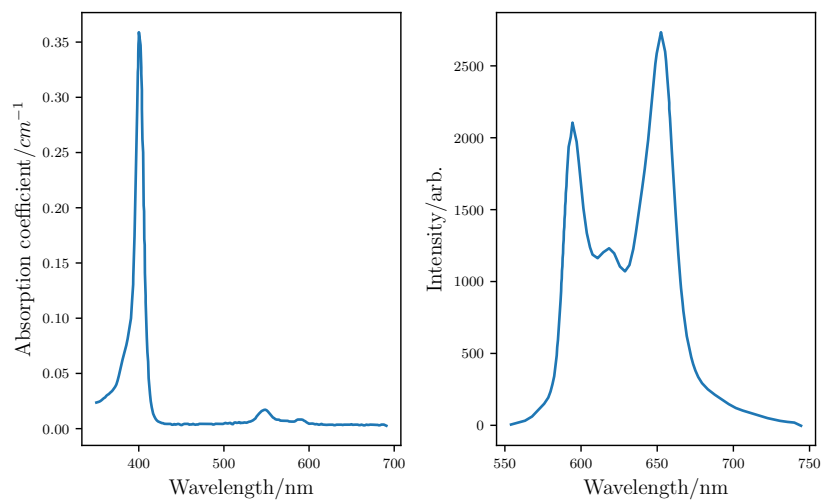
8

Figure 1.7: *Optical properties of Coproporphyrin III. The figure on the left shows the absorption coefficient as a function of wavelength. The figure on the right shows the emission spectrum as a function of wavelength.*
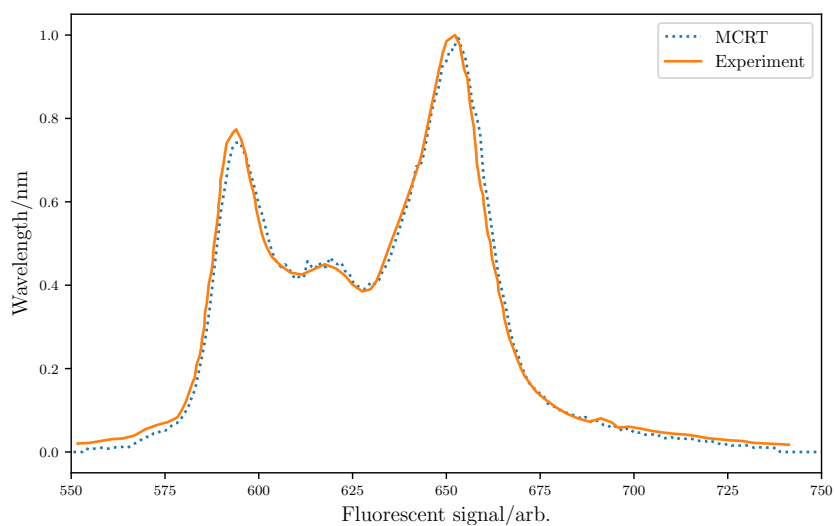

Figure 1.8: *Validation of florescence modelling technique ***fix labels, they are back to front****

1.4 Nelder-Mead Method

The Nelder-Mead (NM) method is an algorithm for unconstrained optimisation. The algorithm is based upon iteratively updating a simplex. A simplex is a structure in $n-dimensional$ space, consisting of $n+1$ points that are not in the same plane. Therefore in 1D, the simplex is a line, in 2D a triangle, in 3D a tetrahedron, etc.. The Nelder-Mead method is a gradient free method, meaning that it does not require derivatives to be calculated and that the search space does not need to be smooth. This makes it ideal for problems where derivates are not able to be computed easily, or the search space is not smooth. However the NM method can also get stuck at local minima so care must be taken to avoid this.

The NM algorithm works by removing the worst vertex of the simplex and replacing it with a 'better' vertex calculated via a number of different operations. These operations can be seen in Fig. 1.9.

The first step of the NM method is to sort the initial vertices according to their fitness. For $n = 2$, we define x_w as the 'worst' point, x_l and the 'lousy' point, and x_b the 'best' point, such that $f(x_b) \leq f(x_l) \leq f(x_w)$, where $f(x)$ is evaluating the 'fitness' of a point x. The fitness function varies from problem to problem, and usually takes the form of the function that is being optimised.

With the vertices sorted, the centroid of the simplex is calculated as in Eq. (1.17). The centroid is the mean of all the vertices bar the 'worst' point.
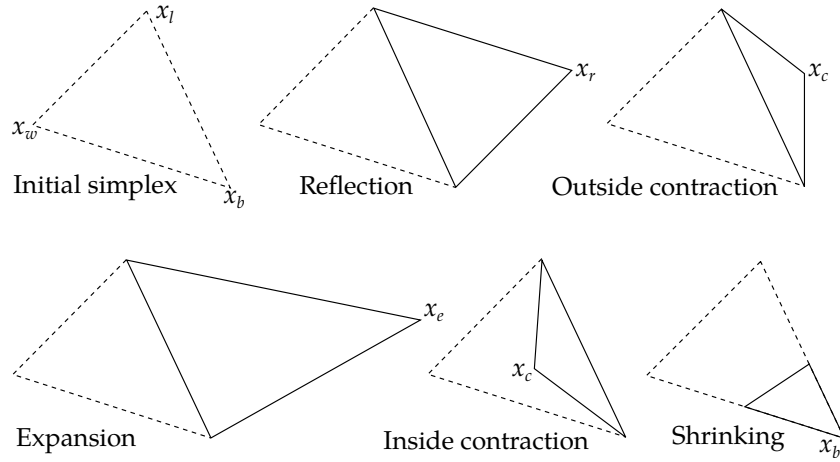

Figure 1.9: *Operations that can be preformed on a simplex for $n = 2$.*

The next step is to move the simplex via a reflection. To calculate the new vertex via reflection Eq. (1.18) is used, where α is the reflection factor. If this new point, x_r, is better[‡] than the current 'best' point then we calculate a new point in the same direction but further using the expansion operation Eq. (1.19), where γ is the expansion factor. If this new point, x_e, is better than the 'best' point then we replace x_w with x_e and start the process again. However is x_e is not better than the 'best' point, then we discard it and replace the worst point with x_r the reflected point.

If when calculating x_r, we find that is worse than the 'best' point, we then check if x_r is better than the 'lousy' point. If x_r is better than x_l then we replace the 'worst' point and start

---

[‡]Here better means the point has a lower fitness score

the process again. However if the x_r is worse than x_l, we then compare it to the 'worst' point. If x_r is better than the 'worst' point then we preform and inside contraction Eq. (1.21), where β is the contraction factor. If this new point, x_{ic}, is better than the 'worst' point then we keep it, otherwise we preform the shrink operation, shrinking the whole simplex around the 'best' point.

If x_r is not worse than the 'worst' point then we preform an outside contraction Eq. (1.20). This computes a new point x_{oc}. If x_{oc} is better than x_w, then we keep it, otherwise again we shrink around the 'best' point.

The process described above is summarised in Fig. 1.10. Standard values for the factors are: $\alpha = 1$, $\beta = \frac{1}{2}$, and $\gamma = 2$. Though in practice these values are adjusted for the problem at hand.

$$c = \frac{1}{n} \sum_{i=1, i \neq w}^{n+1} x_i \tag{1.17}$$

$$x_r = c + \alpha(c - x_w) \tag{1.18}$$

$$x_e = c + \gamma(x_r - c) \tag{1.19}$$

$$x_{oc} = c + \beta(x_r - c) \tag{1.20}$$

$$x_{ic} = c + \beta(x_w - c) \tag{1.21}$$

As the Nelder-Mead method has no inbuilt convergence criteria, this must be added. We use two different criteria based upon simplex size, and vertex fitness. The criteria for the simplex size is as; The size of the simplex is calculated using Eq. (1.22):

$$size = \sum_{i=1}^{n+1} |p_i - p_{i+1}| \tag{1.22}$$

Where p_i and p_{i+1} are vertices in the simplex that are connected by an edge. If the size of the simplex falls below a pre-set value, then we preform a factorial test to see if the simplex should be restarted or if the algorithm should terminate. The factorial test checks the space around the current simplex to ensure that we have converged to a global minima. If the check fails then the algorithm is restarted with the current best point kept, and new vertices generated.

The other convergence criteria is the a check to see if the best point is 'good enough'. The current best point is compared to a pre-set fitness value. If the best point is better than the pre-set value then the algorithm terminates.
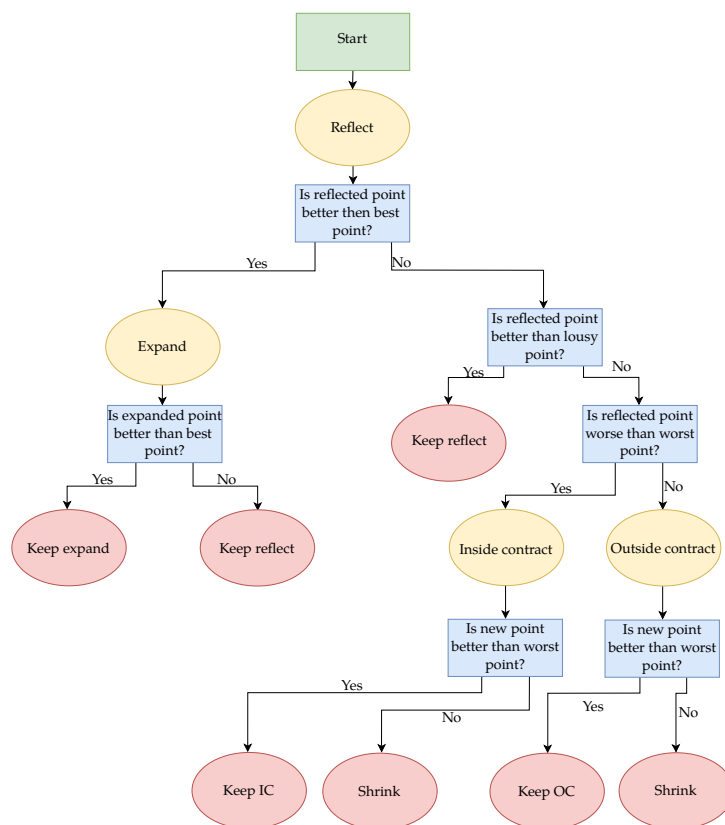
Figure 1.10: *Nelder-Mead decision tree*

1.5 Validation

The NM method was coded in Fortran, so that it could be easily interfaced with the MCRT code developed as part of this thesis. To test that the method works as intended a number of trial functions were tested, see Table 1.3. This was achieved by selecting an initial simplex, and the method allowed to iterate until it converged. The results of this are shown in Fig. 1.11.
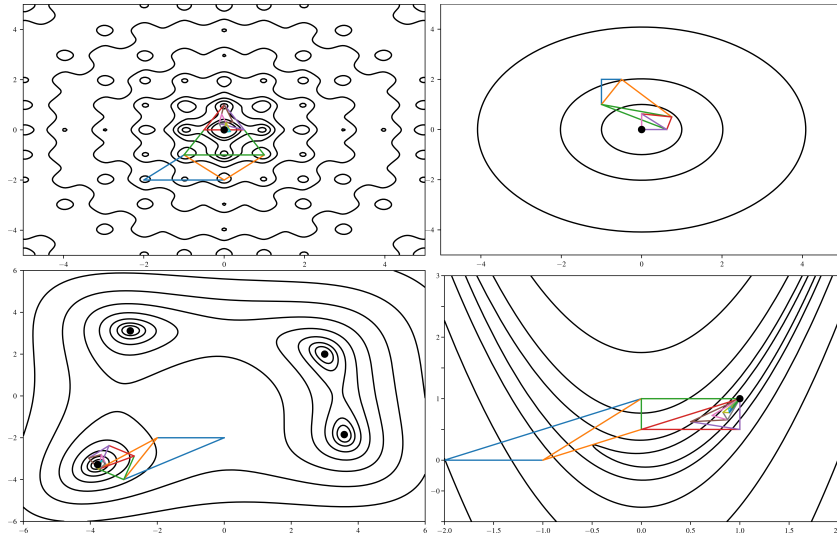

Figure 1.11: *Contour plots of test functions with Nelder-Mead simplexes over plotted. Top left is the Ackely function, top right is the sphere function, bottom left is the Himmelblau's function, and the bottom right is the Rosenbrock function. Blue simplex is the initial simplex, and the large black dots represent the Global minima.*

Some of these functions (Sphere, and Rosenbrock's) can also be extended to arbitrary dimensions. These functions were used to check that the NM method works as intended in these higher dimensions where the NM method will primarily be used in this thesis.

To ensure that the NM method can be used to find the unknown concentrations of the autoflurophores, we test the method with a known model. This model consists of three different fluorophores: NADH (nicotinamide adenine dinucleotide), FAD (flavin adenine dinucleotide), and a fictitious fluorophore that has similar properties to NADH and tyrosine, such that the excitation

Name	Formula	Global Minumum
Sphere	$x^2 + y^2$	$f(0,0) = 0.$
Rosenbrock	$(a-x)^2 + b(y-x^2)^2$	$f(1,1) = 0.$
Ackely	$-20 \exp\left[-0.2\sqrt{0.5\left(x^2+y^2\right)}\right] -$ $\exp\left[0.5\left(\cos 2\pi x + \cos 2\pi y\right)\right] + e + 20$	$f(0,0) = 0.$
Himmelblau's	$(x^2 + y - 11)^2 + (x + y^2 - 7)^2$	$f(3,2) = 0.,$ $f(-2.805118, 3.131312) = 0.,$ $f(-3.779310, -3.283186) = 0.,$ $f(3.584428, -1.848126) = 0.$

Table 1.3: *Table of standard test functions for numerical optimisation.*

spectrum is that of NADH and the emission spectrum is that of tyrosine. The three fluorophores are distributed in the stratum corenum (NADH), epidermis (FAD), and the papillary dermis (fictitious). The concentration in these layers is such that the bulk optical properties are not affected: NADH has a concentration of 1.05 μM, FAD 0.525 mM, and the fictitious fluorophore has a concentration of 0.125 mM. The fitness function chosen to check whether the NM method is converging is as:

$$fitness = \sum_{i=1}^{n}(x_i - m_i)^2 \tag{1.23}$$

Where x_i is a data point at a wavelength λ_i produced by the MCRT, and m_i is a data point in the model at a wavelength λ_i.

As many models need to be run in order to determine whether a global maxima has been reached using the NM method and that the fluorophore concentration is low, means that many packets need to be run to achieve a good single to noise ratio. These two constraints result in a computational load that is infeasible to run. Therefore the MCRT algorithm has to be computationally efficient in order to arrive at an answer within a reasonable time. To this end the 3D skin model is shrunk to a 1D model so that the optical integration routine can efficiently move the photon through the simulated medium. The optical properties of the incident wavelength are also stored so that when a new photon is started the optical properties can easily be adjusted without need for any calculation. Finally a filter is employed on the output fluorescence spectrum to smooth the noise out. The filter used is a SavitzkyGolay filter. This filter fits multiple low-degree polynomials to the subsets of the output, thus smoothing the data.
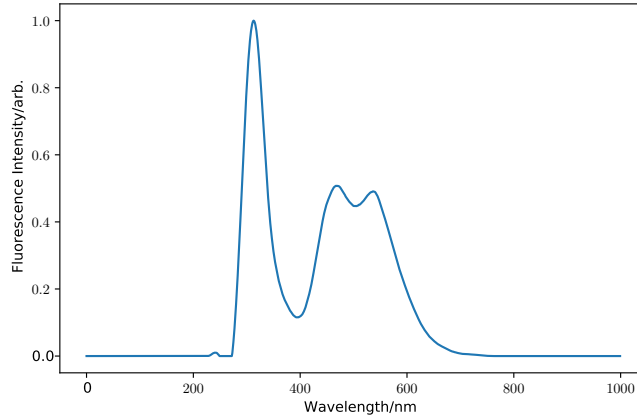

Figure 1.12: *Example of toy model for testing NM method. The three peaks correspond to the fictitious fluorophore, NADH, and FAD respectively.*

The above model is first run through the MCRT to get an output target spectrum. We then test the NM method for $n = 2$ and $n = 3$.

1.6   Results

Before running the NM method on the experimental data, the fluence of the input and fluorescence light is analyses alongside the location as a function of depth of the fluorescent light.

Figure 1.13 show the fluence as a function of depth for the indicent UV light. The figure shows that most of the incident light is contained within the top three layers, with little getting to the Reticular dermis, with none reaching the Hypodermis.

Figure 1.14 shows the fluence of detected fluorescent light (see **??** for discussion of how this is tracked.). The figure shows that the fluence is highest in the Papillary dermis this is due to a number of reasons. First the refractive indices of the layers are different, this can lead to light getting "trapped" in a layer as it maybe reflected of the layer boundary. Secondly, fluorescent light is emitted isotropically which means that fluorescent light emitted in the upper layers of the skin, may be emitted in the direction of the Papillary dermis. Finally the optical properties also have an effect on the detected light fluence. ***expand on this more once I have plotted the optical properties ***
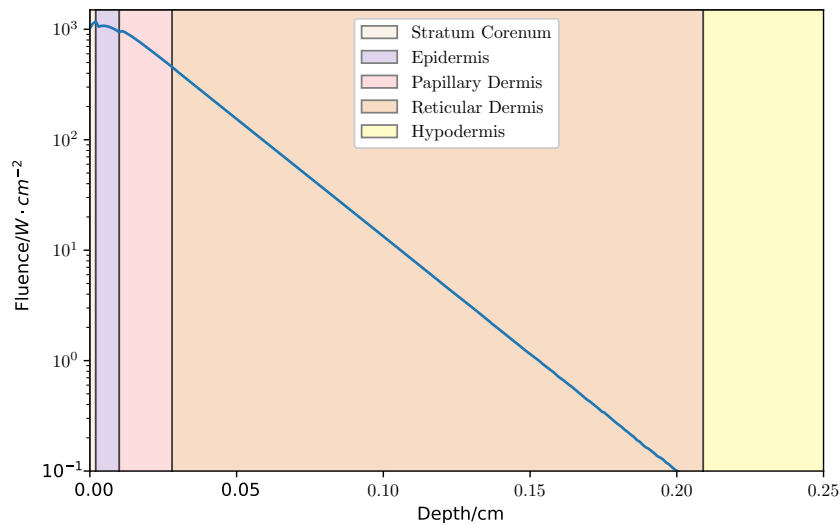

Figure 1.13: *Penetration of UV radiation as a function of depth.*

1.7 Discussion

1.8 Effect of Tissue Optics on Fluorescent Signal

One of the problems in using autofluroescence as a biomarker for various diseases is that information about which fluorophore you are measuring can be hard blah blah

use eem

fad from diff layers nadh from different layers

1.9 Future Work

1.10 Conclusion

We have presented out code, AmoebaMCRT, which combines the Nelder-Mead method and MCRT in order to determine the concentrations of naturally occurring fluorophores in human skin.
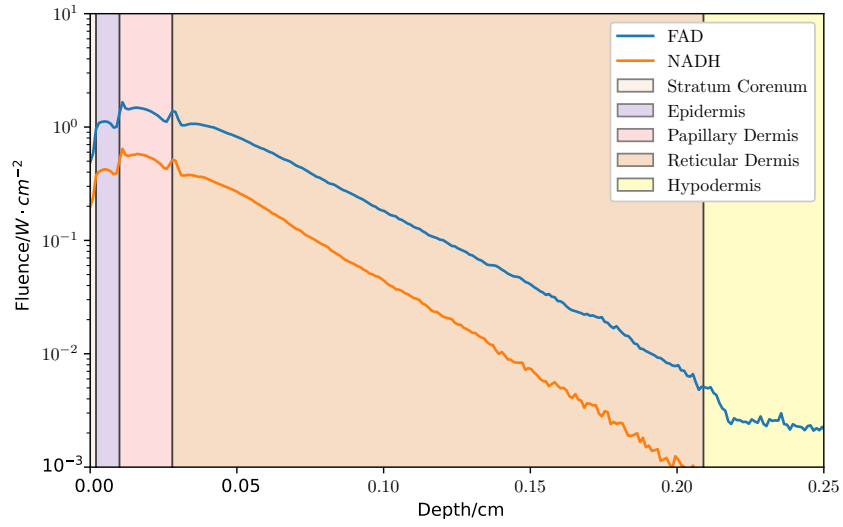
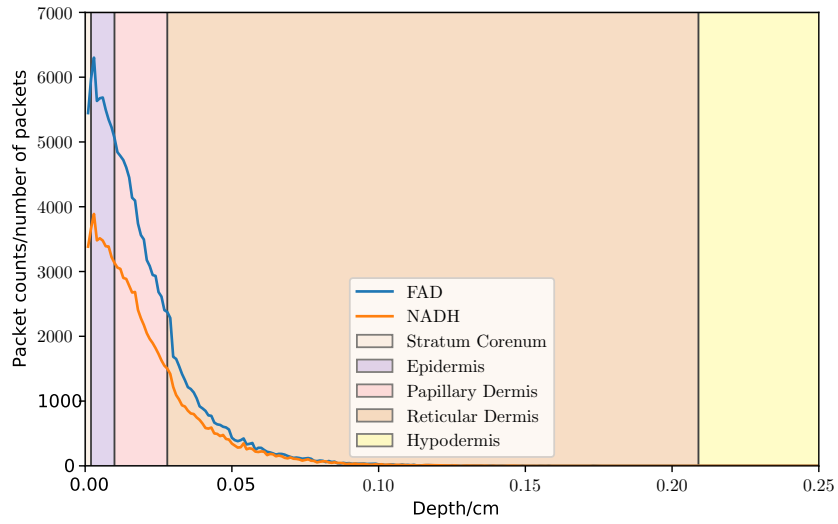**Figure 1.14:** *Penetration of UV radiation as a function of depth.*

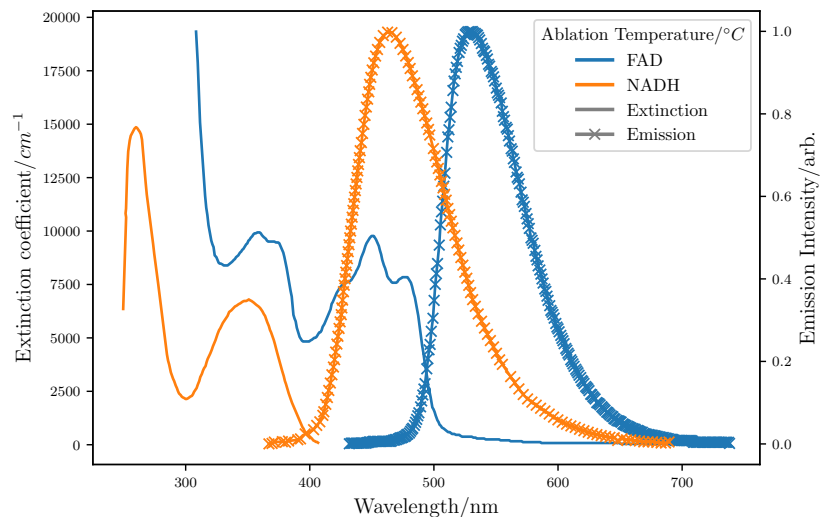**Figure 1.15:** *Penetration of UV radiation as a function of depth.*

Figure 1.16: _Penetration of UV radiation as a function of depth._

Bibliography

[1] World Health Organisation. *Cardiovascular diseases (CVDs)*, 17 May 2017 (accessed June 16, 2019). https://www.who.int/en/news-room/fact-sheets/detail/cardiovascular-diseases-(cvds).

[2] Prachi Bhatnagar, Kremlin Wickramasinghe, Elizabeth Wilkins, and Nick Townsend. Trends in the epidemiology of cardiovascular disease in the uk. *Heart*, 102(24):1945–1952, 2016.

[3] Nikiforos Kollias, Robert Gillies, Michael Moran, Irene E Kochevar, and R Rox Anderson. Endogenous skin fluorescence includes bands that may serve as quantitative markers of aging and photoaging. *Journal of investigative dermatology*, 111(5):776–780, 1998.

[4] S. Prahl. *Tabulated Molar Extinction Coefficient for Hemoglobin in Water*, 1999 (accessed June 15, 2019). https://omlc.org/spectra/hemoglobin/summary.html.

[5] S. Prahl. *Bilirubin*, 2017 (accessed June 15, 2019). https://omlc.org/spectra/PhotochemCAD/html/119.html.

[6] S. Prahl. *Beta-carotene*, 2017 (accessed June 15, 2019). https://omlc.org/spectra/PhotochemCAD/html/041.html.

[7] Iyad Salam Saidi et al. *Transcutaneous optical measurement of hyperbilirubinemia in neonates*. PhD thesis, Rice University, 1992.

[8] Steven L Jacques. Optical properties of biological tissues: a review. *Physics in Medicine & Biology*, 58(11):R37, 2013.

[9] Jose A Iglesias-Guitian, Carlos Aliaga, Adrian Jarabo, and Diego Gutierrez. A biophysically-based model of the optical properties of skin aging. In *Computer Graphics Forum*, volume 34, pages 45–55. Wiley Online Library, 2015.

[10] C. Campbell. *Under the skin: Monte Carlo radiation transfer modelling of photodynamic therapy*. PhD thesis, School of Physics and Astronomy, University of St Andrews, 2016.

[11] Aravind Krishnaswamy and Gladimir VG Baranoski. A biophysically-based spectral model of light interaction with human skin. In *Computer Graphics Forum*, volume 23, pages 331–340. Wiley Online Library, 2004.

[12] I.V. Meglinski and S.J. Matcher. Quantitative assessment of skin layers absorption and skin reflectance spectra simulation in the visible and near-infrared spectral regions. *Physiological Measurement*, 23(4):741, 2002.

[13] C Louise Campbell, Craig Christison, C Tom A Brown, Kenneth Wood, Ronan M Valentine, and Harry Moseley. 3d monte carlo radiation transfer modelling of photodynamic therapy. In *Biophotonics South America*, volume 9531, page 95311H. International Society for Optics and Photonics, 2015.